NASA DEVELOP National Program
Alabama – Marshall

Summer 2024

Peruvian Amazon Ecological Conservation

Assessing Land Cover Changes in the Peruvian Amazon to Identify Exploitative Agriculture Using NASA Earth Observations and PerúSAT-1

DEVELOP Technical Report

August 9th, 2024

Beck De Fazio, Analytical Mechanics Associates (Project Co-Lead)
Brian Arruda, Analytical Mechanics Associates (Project Co-Lead)
Margaret Cox, Analytical Mechanics Associates
Ashley Laveriano, Analytical Mechanics Associates

Advisors:
Vanesa Martín, NASA SERVIR Science Coordination Office (Science Advisor)
Stephanie Jiménez, NASA SERVIR Science Coordination Office (Science Advisor)
Natalia A. Bermudez, NASA SERVIR Science Coordination Office (Science Advisor)
Jacob Abramowitz, NASA SERVIR Science Coordination Office (Science Advisor)
Dr. Jeffrey Luvall, NASA Marshall Space Flight Center (Science Advisor)
Dr. Robert Griffin, University of Alabama in Huntsville (Science Advisor)

Lead:
Cristina Villalobos-Heredia (Alabama – Marshall)

1. Abstract

Perú aims to preserve Amazon forests that support biodiversity, global carbon storage, and ecosystem regulation. To monitor progress, forested sites are tracked for maintaining at least 30% of baseline tree cover extent. NASA DEVELOP partnered with Comisión Nacional de Investigación y Desarrollo Aeroespacial (CONIDA) and Organismo de Evaluación y Fiscalización Ambiental (OEFA) to quantify deforestation due to palm oil plantation expansion in Ucayali and Loreto between January 2017 and December 2023. Using changes in the Enhanced Vegetation Index (EVI) and Normalized Difference Vegetation Index (NDVI) as proxies for vegetative health, our results revealed a decline in vegetation greenness associated with deforestation and/or agriculture. Using the Landsat series, our tropical Continuous Change Detection and Classification with Spectral Mixture Analysis (CCDC-SMA) estimated 2165.2 km² deforested from 2000 – 2023, with two case studies falling below 30% forest cover by 2023. We explored the feasibility of using PerúSAT-1, a higher resolution imager (up to 1-meter resolution panchromatic imaging and up to 2-meter resolution multispectral imaging) for continuous forest monitoring, and validated the CCDC-SMA results with a supervised classification using high-resolution PerúSAT-1 imagery. Trends in deforestation were consistent across CCDC-SMA and the supervised classification. The classification estimated a 15.3% decrease in natural forest cover from 2018 – 2023. The main limitation of the supervised classification was the temporal resolution of PerúSAT-1 data.

Key Terms

Landsat, PerúSAT-1, CCDC-SMA, deforestation, Peruvian Amazon, palm oil plantation, supervised classification

2. Introduction

2.1 Background Information

Land use practices are a key driver of climate outcomes and can contribute to negative environmental stress or have the potential to promote the stabilization of local, regional, and global climates. The Amazon is a critical carbon sink, with 257 estimated tons of carbon stored in one hectare of the Amazon rainforest (McCarthy, 2020; The Amazon We Want, 2021). Beyond carbon sequestration, the Amazon hosts 10% of the world's species (Flores et al., 2024), highlighting its role as a critical ecosystem. There is direct empirical evidence that the Amazon is losing resilience due to agriculture, logging, and development (Boulton et al., 2022; Smith et al., 2022), risking future dieback with profound implications for biodiversity, carbon storage, and climate change (Armstrong McKay et al., 2022).

Between 2000 and 2020, South America experienced the highest rate of net forest loss in the world (Intergovernmental Panel on Climate Change, 2023). The expansion of agriculture within the Amazon continues to promote further deforestation. Accordingly, palm oil operations are spreading across South America due to increased global vegetable oil demand (Furumo & Aide, 2017). Peru holds the second-largest forest reserve suitable for palm oil expansion in South America (Furumo & Aide, 2017). With a high productivity to low land use ratio of 5 tons/ha, palm oil farming is more economically feasible and scalable compared to other commodity crops in the region (Herdiansyah et al., 2020). Peru formally recognized palm oil as a commodity crop of national interest in 2000 (Glinskis & Gutierrez-Velez, 2019) and this led to Peru becoming a net exporter through a series of intentional agricultural laws (Lesage et al., 2021).

Small scale agriculture has historically been noted as a major contributor to discourse surrounding deforestation; however, evidence shows industrial monoculture clears more primary rainforest compared to smallholder farms (Ravikumar et al., 2017). Between 2000 and 2010, 72% of total palm oil expansion occurred on Peruvian forest land (Gutierrez-Velez et al., 2011). These two main stakeholders, smallholding farmers and industrial companies, raise or prompt concern over the environmental externalities of palm oil expansion, such as habitat fragmentation and biodiversity loss (Azhar et al., 2017), resulting in social tensions between the two. These impacts have been observed in Ucayali, Perú, a region with a strong palm oil presence, where communities have experienced land disputes and displacement, prompting concerns from

locals (Bennett et al., 2018; Bennett et al., 2019). Such environmental and social externalities highlight the need for remote sensing in monitoring the environmental impacts of palm oil activity and expansion. A common challenge to detecting palm oil is their rapid growth development into a dense canopy, making them spectrally similar to other vegetative covers (Gutierrez-Velez & DeFries, 2013). Other studies have attempted to classify palm oil plantations through spectral angle mapping of multispectral data (Shafri et al., 2011), combining panchromatic or NIR bands (Thenkabail et al., 2004), and manual digitization of oil palm plantation based on known patterns of spectral reflectance (Carlson et al., 2012). If applied effectively and collaboratively, remote sensing can help users monitor and mitigate uncontrolled palm oil expansion (Chong et al., 2017), and ease the hardships caused by inaccessibility due to dense vegetation and terrain.

2.2 Project Partners and Objectives

The Comisión Nacional de Investigación y Desarrollo Aeroespacial (CONIDA) and the Organismo de Evaluación y Fiscalización Ambiental (OEFA) are two organizations at the forefront of leveraging remote sensing technology to elucidate the presence of palm oil in the Peruvian Amazon. CONIDA operates under the Peruvian Ministry of Defense as technical experts of research and development in space science and technology. In September 2016, CONIDA launched and currently operates Peru's first satellite, PerúSAT-1 (CONIDA, 2024). PerúSAT-1's New AstroSat Optical Modular Instrument (NAOMI) is a higher resolution imager with up to 1-meter resolution panchromatic imaging and up to 2-meter resolution multispectral imaging. NAOMI on PerúSAT-1 has a variable swath width from 10 km to 60 km. The satellite is in sun-synchronous orbit, is pointable, and can revisit any location within Peru every three days (eoPortal, 2016). CONIDA grants early access to conservation organizations to "boost efforts related to near real-time deforestation monitoring", leveraging Perú-SAT-1's capabilities towards greater environmental welfare (Villa & Finer, 2018). OEFA, on the other hand, operates under the Peruvian Ministry of the Environment to evaluate environmental impacts across the country (OEFA, 2024). OEFA promotes environmental compliance and aims to balance environmental protection with economic activity. They have a legal imperative to ensure that 30% of land suitable for agriculture in the Amazon is preserved and maintained as forest cover as per Title 5, Article 25 of the nation's forestry and wildlife laws (Decreto Legislativo Nº 1090 - Ley Forestal y de Fauna Silvestre, 2008). Their interest in future monitoring of palm oil plantation expansion and deforestation in the Peruvian Amazon called for a more robust time series change detection analysis. Prior to this project, OEFA was limited to classifying land use and land cover change using PerúSAT-1 for a single year; therefore, we conducted a project exploring the feasibility of utilizing Perú-SAT for continuous land monitoring across a multi-year time span. Our objectives for this project were: (1) quantifying deforestation in the Peruvian Amazon using the Landsat series and (2) classifying and validating change detection using high-resolution Perú-SAT-1 imagery. The project built upon OEFA's capacity to detect palm oil plantation expansion over a multi-year span using Earth observations. Additionally, the DEVELOP project aimed to expandthe partner's capacity to operationalize and integrate Perú-SAT-1 imagery into their current monitoring efforts.

2.3 Study Area and Period

Located in north-central Perú, our study includes parts of Loreto and Ucayali. The study area is composed of about 6,800 square kilometers of land and consists of four smaller case studies, where land has been allocated for palm oil plantation use (Figure 1). The study area's associated ecoregion is mostly lowland jungle, with elevation ranging from 80 to 400 meters, making it conducive for palm cultivation (Peru Explorer, 2024). Our study period ranges from January 2017 – December 2023, in alignment with PerúSAT-1 becoming operational in late 2016. Starting in 2017 and capping our study in 2023 ensured data availability that covered complete years.

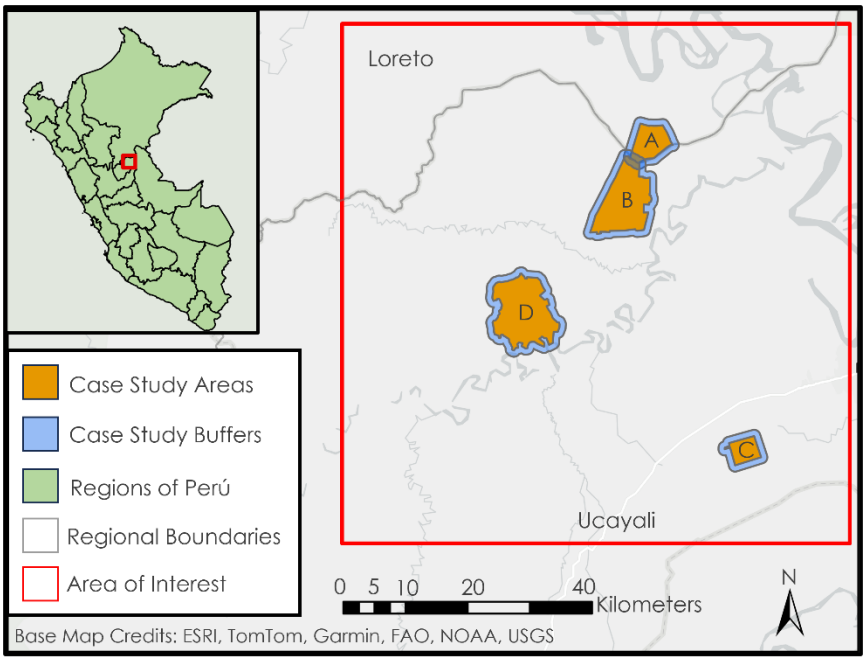

Figure 1. Map of the study area located in Peru's administrative regions of Loreto and Ucayali

3. Methodology

3.1 Data Acquisition

For this project, we utilized a combination of ancillary data provided by our partners, open-source data, and PerúSAT-1 imagery. Our partners provided us with a shapefile outlining the study area and four case studies within it of currently monitored plantations to focus our analysis scope within the larger area or interest. We labeled these case studies A, B, C, and D for clarity (Figure 1). To capture a more holistic understanding of the deforestation dynamics around these areas, we analyzed a 1-kilometer buffer, or edge zone, around each case study area. Each case study represents zones permitted for agricultural use and these zones are required to maintain 30% as natural forest.

In order to perform a vegetative land cover analysis, we used the red and near infrared bands of Landsat 8 Operational Land Imager (OLI) and Landsat 9 OLI-2 to calculate the Normalized Difference Vegetation Index (NDVI; Rouse et al., 1973) and the blue, red and near infrared bands of the same sensors to calculate Enhanced Vegetation Index (EVI; Huete et al., 2002). We accessed Landsat imagery via the Google Earth Engine catalog for the years 2017 and 2023 (Table 1). To quantify natural forest loss by year over the entire study period, we acquired Landsat 4 & 5 Thematic Mapper (TM), Landsat 7 Enhanced Thematic Mapper Plus (ETM+), and Landsat 8 OLI Collection 2 surface reflectance products covering our study region via the GEE catalog, filtering the imagery from January 1, 2000, – December 31, 2023 (Table 1). We selected the broader Landsat series given its moderate spatial resolution of 30 meters and consistency in global monitoring over several decades. For a land cover classification with a smaller study area and a greater accuracy, we acquired PerúSAT-1 imagery through our partner, CONIDA, that captured the study area multiple times between June 2018 – December 2023 (Table 1). PerúSAT-1 is an optical Earth observation system that provides a spatial resolution greater than the Landsat series: 0.7 meters for panchromatic image and 2.8 meters for multi-spectral image data. Acquiring PerúSAT-1 data allowed us to conduct a high-resolution supervised classification of land cover including palm oil agriculture over the study period. It includes blue, green, red, and near-infrared bands and the satellite captures images from about a perpendicular angle due to its tilting capabilities and captures swaths with widths between 10km-60km (eoPortal, 2016). Acquiring PerúSAT-1 data allowed us to conduct a high-resolution supervised classification of land cover including palm oil agriculture over the study period.

Table 1
Earth Observations Acquired

Platform and Sensor	Processing Level/Data Product	Data Provider	Parameter(s)
Landsat 4 TM	Collection 1 Surface Reflectance	Earth Engine Data Catalog/USGS	Surface Reflectance
Landsat 5 TM	Collection 1 Surface Reflectance	Earth Engine Data Catalog/USGS	Surface Reflectance
Landsat 7 ETM+	Collection 1 Surface Reflectance	Earth Engine Data Catalog/USGS	Surface Reflectance
Landsat 8 OLI	Level 2, Collection 2, Tier 1 Surface Reflectance	Earth Engine Data Catalog/USGS	Surface Reflectance, Normalized Difference Vegetation Index (NDVI), Enhanced Vegetation Index (EVI)
Landsat 9 OLI-2	Level 2, Collection 2, Tier 1 Surface Reflectance	Earth Engine Data Catalog/USGS	Surface Reflectance, Normalized Difference Vegetation Index (NDVI), Enhanced Vegetation Index (EVI)
PerúSAT-1	N/A	CONIDA	Radiance

3.2 Data Processing

3.2.1 NDVI & EVI

To understand how much deforestation took place in our study area from 2017 – 2023, we first identified changes in plant cover between 2017 and 2023. We used the difference in Normalized Difference Vegetation Index (NDVI) to get a baseline understanding of vegetative cover (Equation 1; Souza et al., 2005). We then used the difference in the Enhanced Vegetation Index (EVI) to correct for some atmospheric conditions and canopy background noise, which is sensitive to dense vegetation present through the Peruvian Amazon (Equation 2; Matsushita et al., 2007). In both Equations 1 and 2 NIR indicates near-infrared reflectance and RED indicates red reflectance. We mapped these indices by year and calculated total change between 2017 and 2023. We applied a water mask, JRC Global Surface Water Mapping Layers, v1.4, using the "max_extent" band in GEE to mask out noise due to changes in riverbank shifts over time.

$$NDVI = \frac{(NIR - RED)}{(NIR + RED)} \quad (1)$$

$$EVI = \frac{2.5 \cdot (NIR - RED)}{NIR + (2.4 \cdot RED) + 1} \quad (2)$$

3.2.2 CCDC-SMA

We conducted a Continuous Change Detection Classification with a Spectral Mixture Analysis (CCDC-SMA) to evaluate the dynamics of forest loss by year in our study area from January 2000 to December 2023. We acquired a Tropical CCDC-SMA GEE script developed by Dr. Shijuan Chen (Chen et al., 2021) from her publicly available GitHub site. SMA refers to the method of decomposing the spectral signature of a mixed land cover into sub-pixel elements called endmembers; in our case, (1) Green vegetation (GV), (2) Soil, (3) Non-photosynthetic vegetation (NPV), (4) Shade and (5) Cloud. The CCDC-SMA algorithm characterizes

tree cover dynamics by intensifying the spectral signals of forests and filtering out background noise in the data using the Normalized Difference Fraction Index (NDFI; Equation 3; Chen et al., 2021; Souza et al., 2005).

$$NDFI = \frac{GV_{shade} - (NPV + Soil)}{GV_{shade} + (NPV + Soil)} \quad \text{where } GV_{shade} = \frac{GV}{1 - Shade} \tag{3}$$

Without SMA, the CCDC would have used raw spectral bands to identify breakpoints (French et al., 2023). With spectral unmixing, the CCDC looked at sub-pixel components to identify breakpoints and create a harmonic regression model. With each new break, the algorithm generated a new harmonic regression model, ultimately creating a discontinuous series of segments and breaks representing distinct trends in land cover change (See example in Figure 2).

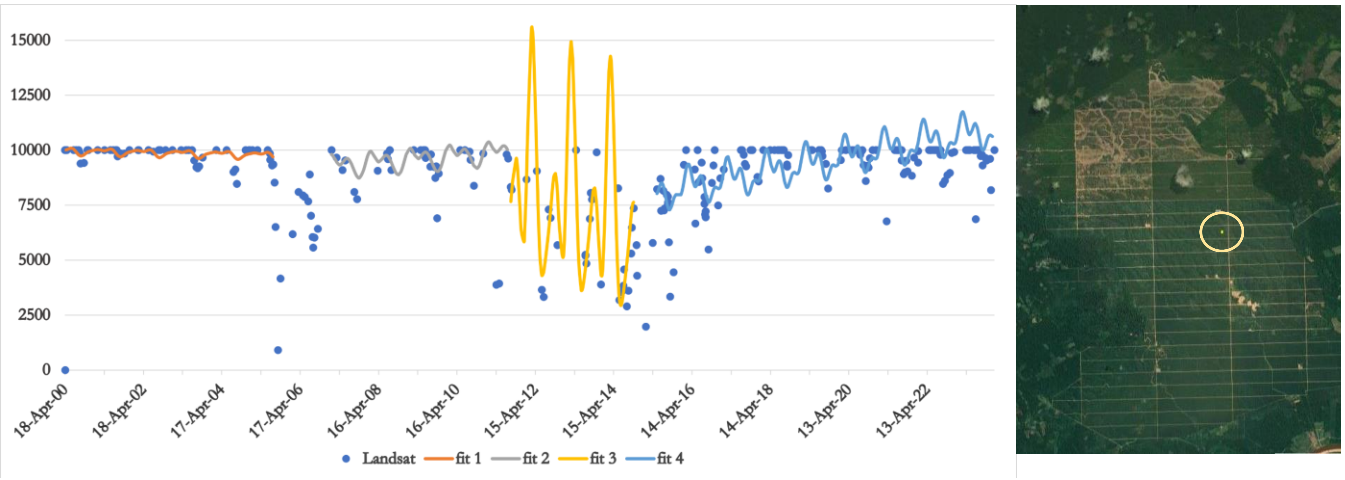

Figure 2. (Left) CCDC-SMA time series showing observed NDFI and resulting harmonic regression models for a 30m x 30m Landsat pixel in case study D, 2000 – 2023. Observed NDFI values cannot exceed 10,000. (Right) Landsat Image via Google Earth Engine with the identified pixel circled in yellow.

The metric that determined the change threshold for the tropics version of CCDC-SMA was: Soil fraction – NDFI. If five consecutive observations exceed the value of the NDFI change threshold, the model flags a disturbance. Changes related to re-growth would not be a disturbance because the value of Soil – NDFI are negative (i.e. in which there is observed soil fraction < predicted soil fraction and the observed NDFI > predicted NDFI). Thus, we assumed that the detected change was related to tree cover loss. In combination with different SMA metrics, different values for the threshold resulted in higher accuracy for different forest types and gradual versus abrupt changes. We assessed the sensitivity of the algorithm to different NDFI change threshold values for our study area, and ultimately decided to stick with the default setting of 2600 as it had the least noise to change ratio.

The creators of the combined CCDC-SMA algorithm (Chen et al., 2021) suggest some default values for other variables, including the consecutive change (5), change probability (.99), and endmember thresholds (Table 2). In consultation with their recommendations and with literature that has utilized CCDC-SMA in similar contexts, we left many of the parameters on their default (Chen et al., 2021; Zhu and Woodcock, 2014; Bullock et al., 2020; Arévalo et al., 2020; Arévalo et al., 2023). To narrow the spatial scope of the data-heavy analysis, the CCDC-SMA algorithm uses two preprocessed inputs from the user, a study region, and a forest mask. For the study region, we used our study area in Loreto and Ucayali identified in the shapefile provided by our partners. For the forest mask, we used the publicly available Global Forest Change dataset in GEE from Hansen et al. (2013), which shows global forest cover at 30-meter spatial resolution between 2000

and 2014. We used the 'tree cover 2000' band from this dataset to exclude unforested land, or pixels with less than 80% tree cover in the year 2000 from the disturbance detection.

Table 2

Parameters for the CCDC-SMA Tropics Application

Parameter Name	**Description**	**Recommended Value**	**Effect of Increasing**
Num of consec	Number of consecutive observations exceeding the threshold to flag a change	5	Less changes detected
NDFI Threshold	The value of Soil – NDFI needed to flag a disturbance Min: 0; Max: 10,000	2600	Less changes detected
Change probability	Threshold on test statistic, which is calculated from the model residuals and follows a chi-square distribution (width of statistical change window)	0.99	Less changes detected
Cloud Mask Threshold	'cfThreshold' is the variable for cloud masking Landsat imagery with less than 5% cloud cover	0.05	Less changes detected

Since our study area is in the tropical Amazon, we chose a CCDC-SMA script specifically calibrated to detect changes in tropical forests. Though the CCDC-SMA is compatible with other software tools and satellites (i.e. Python and Sentinel-1/2), we chose GEE as our processing platform due to our partner's familiarity with the platform and its default language of JavaScript. The analysis used available imagery from the Landsat series (Landsat 4 & 5 TM, 7 ETM+, and 8 OLI) covering our study area from 2000 – 2023.

3.2.3 Supervised Classification

Data processing consisted of converting the raw satellite images listed in Table B1 into a format suitable for analysis. We began with preprocessing, which included radiometric conversion of radiance to top-of-atmosphere reflectance (Figure 3; Equation 4; Updike et al, 2010). This conversion is performed on each of the individual bands of the PerúSAT-1 imagery, including Band 0 (blue), Band 1 (green), Band 2 (red), and Band 3 (near infrared/alpha). This requires the specified spectral band *(i)*, spectral band radiance raster (*RAD*), the Earth-Sun distance at the date of acquisition in Astronomical Units (*SunDist*), the bands irradiance values (*EAI*) and the solar zenith angle in degrees (*SolarZenith*; Table B2).

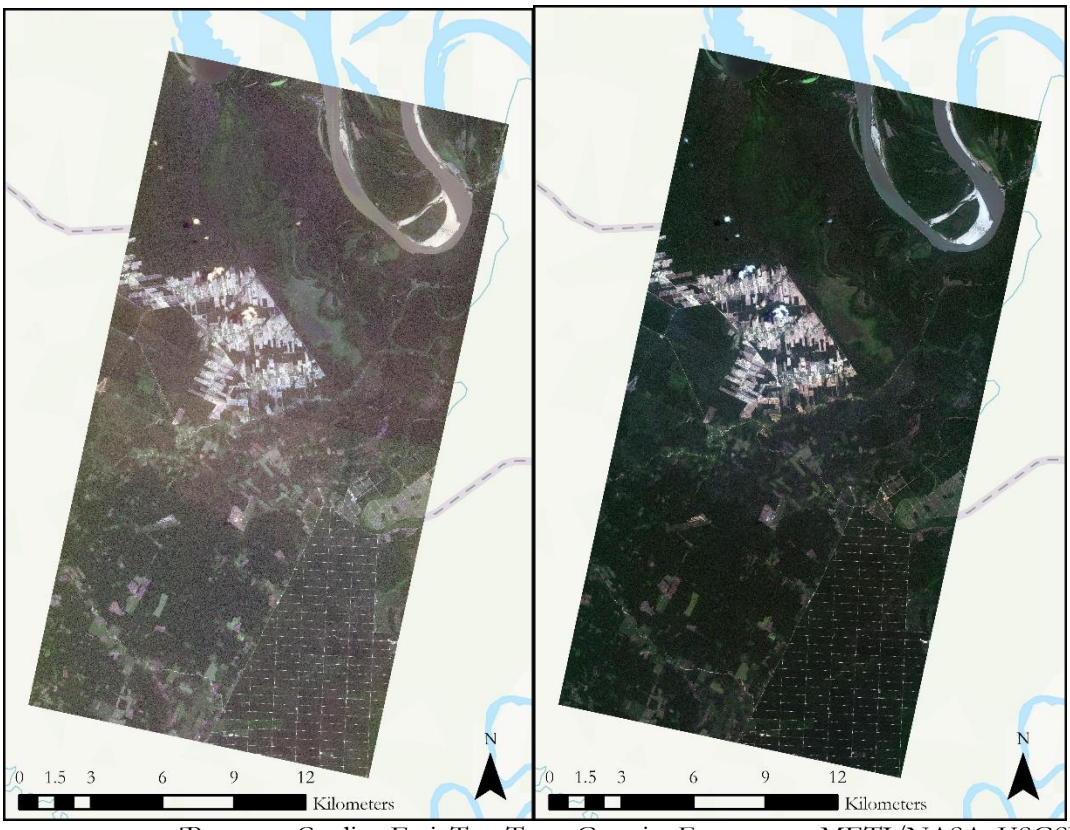

[Basemap Credits: Esri, TomTom, Garmin, Foursquare, METI/NASA, USGS]

Figure 3. (Left)PerúSAT-1 imagery in radiance without any prior processing. (Right) PerúSAT-1 imagery after radiance conversion to top-of-atmosphere reflectance.

$$REF(i) = RAD(i)\frac{\pi \cdot SunDist}{EAI(i) \cdot \cos(SolarZenith)} \quad (4)$$

These values were mostly available in the provided imagery and corresponding metadata files, however Earth-Sun distance had to be calculated manually. This can be calculated once the Julian Date (JD) has been calculated for the given date of acquisition (Updike et al., 2010). We created a Python 3.12 script that automatically generates Earth-Sun distance (d_{ES}) when entering the date and time of image acquisition, reducing the chance of human error in the calculation. The formula for Earth-Sun distance (d_{ES}) is shown in Equation 5, where g is defined as 357.529 + 0.98560028D, and D is defined as $JD - 2451545.0$ (Updike et al., 2010).

$$d_{ES} = 1.00014 - 0.01671 \cdot \cos(g) - 0.00014 \cdot \cos(2g) \quad (5)$$

We also performed minor geolocation correction using the Shift geoprocessing tool in ArcGIS Pro 3.2 to adjust reference point inconsistencies between images. To align the 2023 PerúSAT-1 image with the image from 2018, this image was shifted 1.82 meters on the x-axis, as well as -0.97 meters on the y-axis. Further processing of the imagery included correcting for cloud-cover by incorporating a makeshift cloud mask by implementing separate classifications for clouds and shadows in the imagery during the Supervised Classification geoprocessing tool.

3.3 Data Analysis

3.3.1 Overall Deforestation

We calculated zonal statistics for the disturbed areas to determine the extent of deforestation by the associated first year of change. This included total area, total forested area, percent forested area, area deforested each year for the years 2000 – 2023, and percent of forested area disturbed each year. We also calculated these zonal statistics for each specific case study and surrounding 1-kilometer buffer in the region. We used a forest mask from Hansen et al. (2013) to determine the starting amount of tree cover in the year 2000 as a baseline for change over the study period. We then compared the first year of change maps to high-resolution PerúSAT-1 imagery to determine areas of focus and to better understand the context around, the timing of, and the patterns of forest loss seen in the CCDC-SMA.

3.3.2 Supervised Classification

When creating a supervised classification for land cover using PerúSAT-1 imagery we applied the Support Vector Machine algorithms to the processed images using ArcGIS Pro's Classification Wizard to classify different types of land cover (roads, cleared, agriculture, palm, water, sand, forest, and other non-forest vegetation). We created training data by visually selecting a minimum of 30 polygon features for each class for each year analyzed. This training data was then used to train the classifier and perform the supervised classification analysis. We compared the results of the supervised classification using PerúSAT-1 images in radiance and reflectance (Figure 4). Based on the supervised classification results, we found that the classification performed with the image converted to reflectance had improved contrast and clarity (less noise), and an overall greater accuracy in its classification versus that from the unconverted radiance image. Upon completion of the supervised classification for 2018 and 2023, we then used a pixel count to determine the percentage change of land cover types over the approximate five-year period. Our primary focus in calculating these statistics was quantitatively identifying the depletion of natural forest cover in the classified area.

[Basemap Credits: Esri, TomTom, Garmin, Foursquare, METI/NASA, USGS]

Figure 4. Supervised classification of 2018 PerúSAT-1 imagery (left) and 2023 PerúSAT-1 imagery (right) after being converted from radiance to top-of-atmosphere reflectance. These images show Case Study Area A as well as the northern portion of Case Study B.

4. Results & Discussion

4.1 Analysis of Results

4.1.1 Trends in Deforestation

Green vegetation in our study area, both its thickness and overall health, decreased during our study period, with the magnitude of change in some areas showing signs of total vegetation loss (Figure 5). The change in NDVI illustrates a broader trend in vegetative health decline across our area of interest, with large sections, noticeably to the upper left and lower right of case study areas A and B, highlighting widespread moderate declines during our study period. In the EVI image, the magnitude of change in certain areas is highlighted in the bright yellow color, calling attention to areas where canopy thickness has been reduced or eliminated over the course of the same period (Figure 5).

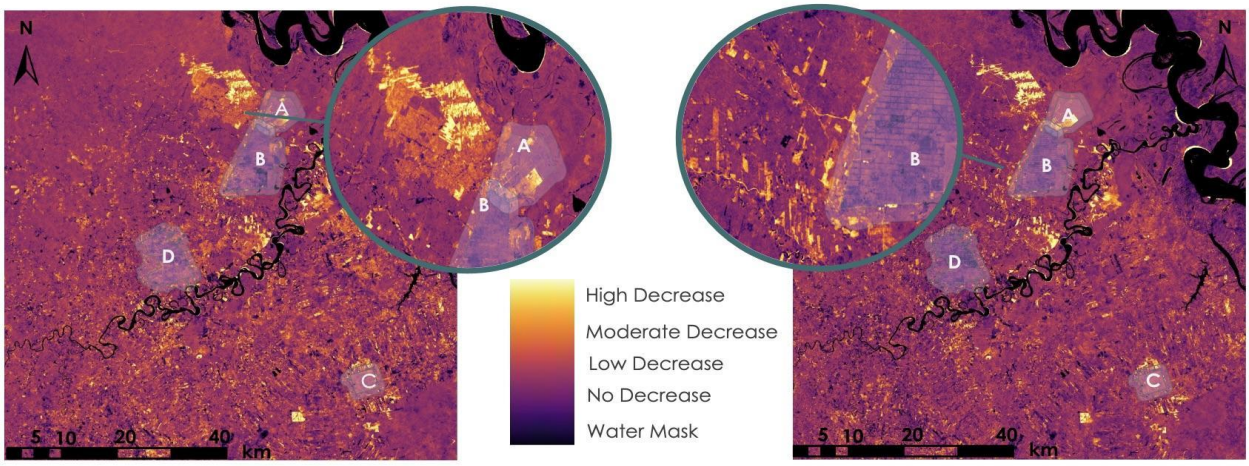

Figure 5. Change in NDVI, 2017-2023 (Left) and change in EVI, 2017-2023 (Right)

Following our tropical CCDC-SMA analysis, we found that 2165.2 square kilometers of forest was lost between 2000 and 2023, which is equivalent to 37.8% of the total forest in the study area that existed in 2000. Within that time period, 8.7% of the total forest loss occurred within the four case study areas. Between 2017 and 2023 alone, approximately 709 square kilometers of forest was disturbed in the study area (Figure A1).

As of 2023, Case Study area A was 82% forest and Case Study area C was 68.20% forest, meaning they are in good standing with the regulation of maintaining 30% forest within each case study/permitted zone. As of 2023 Case Study area B was 12.76% forest and Case Study area D was 25.68% forest (Figure 6). The year 2005 stands out as a major year of forest loss for the entire study area and for study area C, but it may be due to noise (Table 3). Case Study area C had no one particular year with a distinctly high amount of loss. Disturbances associated with 2005 mostly occurred in separate, single instances which are inconsistent with typical patterns of city or palm oil plantation expansion seen over the time period.

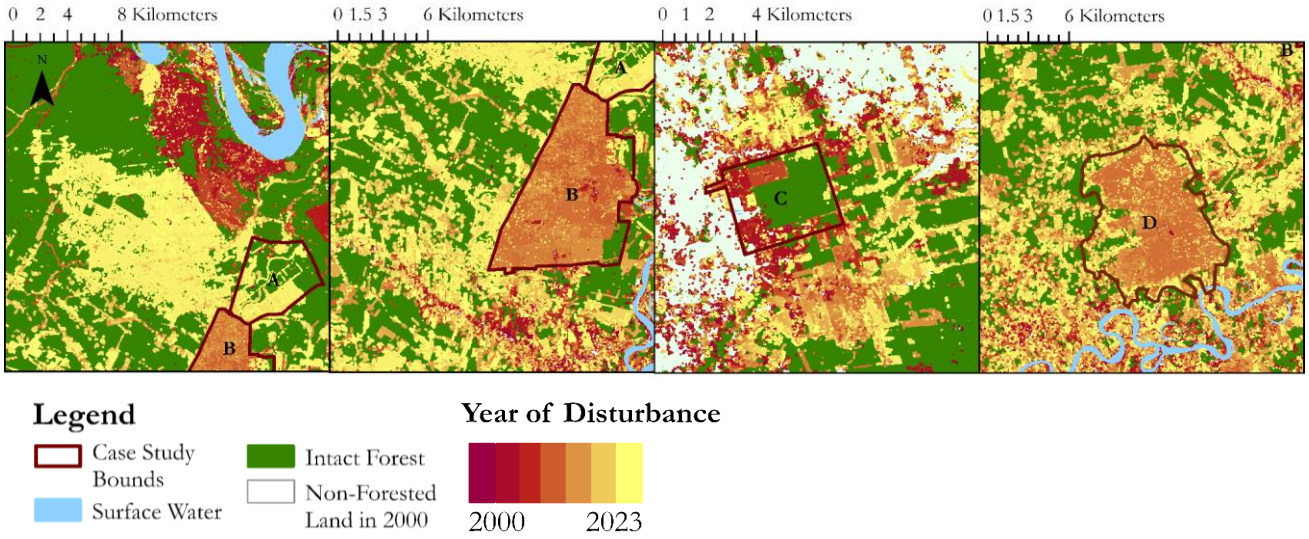

Figure 6. Maps from the CCDC-SMA showing deforestation by year between 2000 – 2023 for each case study (A, B, C, and D from left to right)

Table 3

Results identify the amount of forest still currently intact in each case study and within the area of interest, and the greatest years of deforestation between 2000 – 2023

Area	**% of Area Forested**	**Forest Area Lost (km^2)**	**Greatest Loss Period**
A	82.00	9.20	2021-2023
B	12.76	63.42	2012-2013
C	68.20	5.03	2005*
D	25.68	65.10	2013
AOI	31.94	2165.17	2005*, 2013, 2022

*May be due to noise in the data for that year (e.g., from unmasked cloud contamination)

4.1.2 Supervised Classification

Upon performing supervised classification, we found that natural forest cover decreased by 15.30%, palm plantations remained at about 8.61%, and cleared/developed land increased by 7.20% between 2018 and 2023 in the subregion of Case Study A. As evident in Table 4, the decrease in forest cover coincides with an increase in industrial development and cleared land. Anthropogenic causes associated with creating new agricultural plots explain the forest cover loss despite the % of palm decreasing over time.

Table 4

Results identifying the % of the subregion of Case Study area A made up by each of the classes used in the supervised classification. The difference in (%) between land cover class composition between 2018 and 2023.

Class	**% of Area in 2023**	**% of Area, Difference (2023 - 2018)**
Natural Forest	68.07	-15.30
Palm (agriculture)	8.61	-0.38
Developed/Cleared	10.21	7.20
Non-Forest Vegetation	12.70	11.84
Water/Sand	< 1.0%	-0.02
Clouds/Shadows	< 1.0%	-3.49

4.2 Errors & Uncertainties

While conducting the analysis and exploring the results, we identified several potential sources of uncertainty and error. Since the CCDC-SMA composited imagery from across the Landsat series, there may have been inconsistencies in change detection related to the availability of cloud-free images and differences in sensor functionalities between Landsat ETM+ and Landsat 8 OLI. We chose a relaxed threshold for NDFI that is standard for tropical forests, but this may have led to areas being identified as disturbed when not. A possible example of this was with the year 2005, where we detected a higher amount of disturbance compared to any other year between 2000 – 2023. With a more conservative NDFI threshold value, disturbances associated with 2005 decreased far more than changes in any other year. The limited availability of Landsat data from

the early 2000s compared to the availability after 2015 is a common problem for studies evaluating long-term change. Including Landsat 9 OLI-2 in future datasets would supplement the analysis and improve accuracy.

Additional uncertainties with the supervised classification may be related to PerúSAT-1's satellite data collection processes. There can be issues with capturing certain areas or gaps and inconsistencies caused by the data retrieval methods. For example, the 2023 PerúSAT-1 Imagery was shifted eastward in ArcGIS Pro 1.82 meters on the x-axis and southward about 0.97 meters on the y-axis due to geolocation inconsistencies between the 2018 and 2023 images. This helped overlay the images to retrieve more accurate statistical analysis; however, any alteration of the imagery introduces the opportunity for misalignment and human error.

The limited field validated training data overlapping with the supervised classification area may have led to improper classifications in the training data points that were selected visually from the high-resolution imagery. To assess the accuracy of the supervised classification methodology using PerúSAT-1 imagery, a similar methodology was performed using PerúSAT-1 imagery from 2022 in an area that had accessible validation training points provided to us from our partners (Figure B1). This classification was performed using the classes provided for us in the training points, which do not correspond to the 2018 and 2023 land cover classes we used (Table B5). This additional classification gave us a prospective accuracy of approximately 73.48%, which was calculated using a confusion matrix (Table B3; Table B4). While the accuracy of the classification may seem low, this classification area spanned about 260 km2; classifying such a small area is inherently more difficult and prone to bias due to the smaller sample size. Training data and the diversity of spectral signals captured was limited by the availability of PerúSAT-1 imagery that (1) overlapped the same area and (2) were taken in different years. Another concern was access to relevant imagery, given the low temporal resolution of the imagery, we were unable to look at classification changes for our whole study area and period. This could be improved upon in the future through consistent imagery collection.

4.3 Feasibility & Partner Implementation

This project successfully used Earth observations to quantify and map deforestation and palm oil plantation expansion from 2000 – 2023, building upon our partners' ability to integrate PerúSAT-1 imagery processing and analysis into ongoing monitoring efforts. Our partners can utilize nearly all methods in this study to explore palm oil plantation expansion to enhance their decision-making processes for deforestation monitoring, with the caveat that additional validation data, error assessments, and accuracy measures are needed for official government use.

We found that the CCDC-SMA algorithm is an effective method to identify disturbed forest areas in the tropical regions of the Peruvian Amazon (Figure A2). Using Landsat provides enough images for the CCDC-SMA to assess change over a large time span, map the year of occurrence, and overcome challenges with cloud cover. Although running a tropical CCDC-SMA is a computationally intensive process, the program developed by Chen et al. (2021) allows users to tailor parameters to conditions of their specific study area and to visualize results with disturbance maps and harmonic regressions. This tool is useful for both demonstrating the history of deforestation in the region and predicting areas vulnerable to future loss. The tropical CCDC-SMA highlights potential areas of future forest loss (northwest of Case Studies A & B) that will help inform the partners' focus for future monitoring efforts.

Using PerúSAT-1 imagery for a supervised classification added confidence to the attribution of forest loss to palm oil plantation expansion, given PerúSAT-1's high spatial resolution (relative to Landsat). However, future studies would benefit from enhanced metadata that includes Earth-Sun distance for radiance to reflectance conversions. Additionally, a more precise geolocation of PerúSAT-1 imagery and greater temporal resolution would greatly improve the feasibility of PerúSAT-1 applications in future research. This project's monitoring of forest loss caused by plantation operations will offer a methodology that utilizes and integrates PerúSAT-1 imagery and will help inform our partners' management of exploitative agriculture. Integrating

continuous change detection in a semi-automated monitoring program with high resolution validation data could alert partners to expansion activities and provide proof of agroforestry expansion over time.

5. Conclusions

The team found that NDVI and EVI change maps indicated an overall decrease in green vegetation health from 2017 – 2023 for many areas undergoing forest to agricultural conversion. The CCDC-SMA narrowed in on the decrease in vegetation health due to forest loss, and quantified the total area deforested in the region from 2000 – 2023 as 2165.2 km^2. When evaluating the amount of intact forest in each case study area, we found that Case Study areas A & B contained less than 30% forest as of 2023. Though CCDC-SMA proved to be an effective method for identifying areas of forest loss in the Peruvian Amazon, it could not ascribe that loss to any particular cause. Though we could infer the cause from the history of the region and the visualized deforestation patterns, the supervised classification was successful in classifying distinct changes in Palm Agriculture, Natural Forest Cover, and Developed/Cleared lands in a small area. Our supervised classification using PerúSAT-1 supported our inferences that a decline in natural forest cover corresponds to an increase in cleared/developed lands, or anthropogenic causes for deforestation, such as roads, cleared agricultural plots, and infrastructure from 2018 – 2023 in the observed images. Our results exemplify PerúSAT-1's feasibility in providing land cover classifications and identifying change over time for a small area. These results could be refined and expanded across a much larger area given minor adjustments to improve application feasibility (temporal resolution, geolocation precision, and enhanced metadata). OEFA can use the results from this study to help stakeholders make informed decisions about where and why deforestation occurs, particularly in relation to the growing palm oil industry. Ultimately, this research contributes to the capability of using Earth observations to understand the causes and extent of deforestation in the Peruvian Amazon, providing critical information for future monitoring and mitigation efforts.

6. Acknowledgements

We would like to thank the following individuals for their support:

- OEFA: Marco Miranda Valiente
- CONIDA: José Pasapera, Julian Llanto
- NASA SERVIR Science Coordination Office (Advisors): Vanesa Martín, Stephanie Jiménez, Natalia A. Bermudez, Jacob Abramowitz
- NASA Marshall Space Flight Center (Advisor): Dr. Jeffrey Luvall
- University of Alabama in Huntsville (Advisor): Dr. Robert Griffin

With special thanks to:

- NASA DEVELOP MSFC Center Lead: Cristina Villalobos-Heredia
- NASA SERVIR Science Coordination Office: Christine Evans & Lauren Carey
- NASA DEVELOP Project Coordination: Marisa Smedsrud

Any opinions, findings, and conclusions or recommendations expressed in this material are those of the author(s) and do not necessarily reflect the views of the National Aeronautics and Space Administration.

This material is based upon work supported by NASA through contract 80LARC23FA024.

7. Glossary

CCDC-SMA – Continuous Change Detection and Classification - Spectral Mixture Analysis
CONIDA – Comisión Nacional de Investigación y Desarrollo Aeroespacial
Deforestation – The change from forest to another land cover or land use, such as forest to plantation or forest to urban area
Earth observations – Satellites and sensors that collect information about the Earth's physical, chemical, and biological systems over space and time
Earth-Sun Distance – Approximately one astronomical unit that averages about 93 million miles or 150 million km, utilized in remote sensing to normalize seasonal changes between Earth and Sun

EVI – Enhanced Vegetation Index
GEE – Google Earth Engine
Irradiance – The exchange of energy (in the form of photons) across an area of flat surface per time
Landsat – A collection of Earth-observing satellite missions jointly managed by NASA and the United States Geological Survey
NDFI – Normalized Difference Fraction Index
NDVI – Normalized Difference Vegetation Index
Non-Photosynthetic Vegetation (NPV) – Vegetative cover that does not take part in the photosynthesis process, can include dormant, senescent, dead vegetation, or woody debris of plants
OEFA – Organismo de Evaluación y Fiscalización Ambiental
Palm Oil – Grown in the tropics, the oil palm tree produces high-quality oil utilized in food products, cosmetics, and fuel
PerúSAT– A high-resolution Earth observation satellite launched in 2016 and managed by the Peruvian government and space agency
Remote Sensing – Acquisition of information from a distance via remote sensors on satellites or aircraft
Spectral Signature – Reflected wavelengths detected by a sensor that determines the type of material it reflected from
Supervised Classification – A machine learning method that utilizes pre-determined and labeled training data to define land cover classes within a given image
Temporal Resolution – The time it takes for a satellite to revisit the same location

8. References

Anzualdo, V. I. T., Chavez, F. A., Vega-Guevara, M., Esenarro, D., Cairo, J. V. (2024). Causes and Effects of Climate Change 2001 to 2021, Peru. *Sustainability, 16*(7), 2863. https://doi.org/10.3390/su16072863

Arévalo, P., Bullock, E. L., Woodcock, C. E., & Olofsson, P. (2020). A Suite of Tools for Continuous Land Change Monitoring in Google Earth Engine. *Frontiers in Climate*, *2*. https://doi.org/10.3389/fclim.2020.576740

Arévalo, P., & Olofsson, P. (2023). Interpreting Time Series with CCDC. In J. A. Cardille, M. A. Crowley, D. Saah, & N. E. Clinton (Eds.), *Cloud-Based Remote Sensing with Google Earth Engine: Fundamentals and Applications* (pp. 353–375). Springer International Publishing. https://doi.org/10.1007/978-3-031-26588-4_19

Armstrong McKay, D. I., Staal, A., Abrams, J. F., Winkelmann, R., Sakschewski, B., Loriani, S., Fetzer, I., Cornell, S. E., Rockström, J., & Lenton, T. M. (2022). Exceeding 1.5°C global warming could trigger multiple climate tipping points. *Science*, *377*(6611), eabn7950. https://doi.org/10.1126/science.abn7950

Azhar, B., Saadun, N., Prideaux, M., & Lindenmayer, D. B. (2017). The global palm oil sector must change to save biodiversity and improve food security in the tropics. *Journal of Environmental Management*, *203*, 457–466. https://doi.org/10.1016/j.jenvman.2017.08.021

MBennett, A., Ravikumar, A., McDermott, C., & Malhi, Y. (2019). Smallholder Oil Palm Production in the Peruvian Amazon: Rethinking the Promise of Associations and Partnerships for Economically Sustainable Livelihoods. *Frontiers in Forests and Global Change*, *2*. https://doi.org/10.3389/ffgc.2019.00014

Bennett, A., Ravikumar, A., & Paltán, H. (2018). The Political Ecology of Oil Palm Company-Community partnerships in the Peruvian Amazon: Deforestation consequences of the privatization of rural development. *World Development*, *109*, 29–41. https://doi.org/10.1016/j.worlddev.2018.04.001

Boulton, C. A., Lenton, T. M., & Boers, N. (2022). Pronounced loss of Amazon rainforest resilience since the early 2000s. *Nature Climate Change*, *12*(3), 271–278. https://doi.org/10.1038/s41558-022-01287-8

Bullock, E. L., Woodcock, C. E., Holden, C. E. (2020). Improved change monitoring using an ensemble of time series algorithms. *Remote Sensing of the Environment, 238*. https://doi.org/10.1016/j.rse.2019.04.018

Carlson, K. M., Curran, L. M., Ratnasari, D., Pittman, A. M., Soares-Filho, B. S., Asner, G. P., Trigg, S. N., Gaveau, D. A., Lawrence, D., & Rodrigues, H. O. (2012). Committed carbon emissions, deforestation, and community land conversion from oil palm plantation expansion in West Kalimantan, Indonesia. *Proceedings of the National Academy of Sciences*, *109*(19), 7559–7564. https://doi.org/10.1073/pnas.1200452109

Chen, S., Woodcock, C. E., Bullock, E. L., Arévalo, P., Torchinava, P., Peng, S., & Olofsson, P. (2021). Monitoring temperate forest degradation on Google Earth Engine using Landsat time series analysis. *Remote Sensing of Environment*, *265*, 112648. https://doi.org/10.1016/j.rse.2021.112648

Chong, K. L., Kanniah, K. D., Pohl, C., & Tan, K. P. (2017). A review of remote sensing applications for oil palm studies. *Geo-Spatial Information Science*, *20*(2), 184–200. https://doi.org/10.1080/10095020.2017.1337317

CONIDA. (2024, June 19). *Comisión Nacional de Investigación y Desarrollo Aeroespacial - CONIDA*. gob.pe. https://www.gob.pe/conida

eoPortal. (2016, October 12) *PeruSat-1 Earth Observation Minisatellite*. https://www.eoportal.org/satellite-missions/perusat-1

Flores, B. M., Montoya, E., Sakschewski, B., Nascimento, N., Staal, A., Betts, R. A., Levis, C., Lapola, D. M., Esquível-Muelbert, A., Jakovac, C., Nobre, C. A., Oliveira, R. S., Borma, L. S., Nian, D., Boers, N., Hecht, S. B., ter Steege, H., Arieira, J., Lucas, I. L., Berenguer, E., Marengo, J. A., Gatti, L. V., Mattos, C. R. C., Hirota, M. (2024). Critical transitions in the Amazon forest system. *Nature*, *626*, 555–564. https://doi.org/10.1038/s41586-023-06970-0

French, E., Edulbehram, U., Hughes, S., Arndt, M. (2023). Oregon Coast Range Ecological Conservation: Mapping Recent Logging within Drinking Watersheds of Oregon's Coastal Range to Support Future Resource Management Policies [Unpublished manuscript]. NASA DEVELOP National Program, Massachusetts– Boston.

Furumo, P. R., & Aide, T. M. (2017). Characterizing commercial oil palm expansion in Latin America: land use change and trade. *Environmental Research Letters*, *12*(2). https://doi.org/10.1088/1748-9326/aa5892

Glinskis, E. A., Gutierrez-Velez, V. H. (2019). Quantifying and understanding land cover changes by large and small oil palm expansion regimes in the Peruvian Amazon. *Land Use Policy, 80*, 95-106. https://doi.org/10.1016/j.landusepol.2018.09.032

Gutiérrez-Vélez, V. H., & DeFries, R. (2013). Annual multi-resolution detection of land cover conversion to oil palm in the Peruvian Amazon. *Remote Sensing of Environment*, *129*, 154–167. https://doi.org/10.1016/j.rse.2012.10.033

Gutierrez-Velez, V. H., DeFries, R., Pinedo-Vasquez, M., Uriarte, M., Padoch, C., Baethgen, W., Fernandes, K., & Lim, Y. (2011). High-yield oil palm expansion spares land at the expense of forests in the Peruvian Amazon. *Environmental Research Letters*, *6*(4). https://doi.org/10.1088/1748-9326/6/4/044029

Hansen, M. C., Potapov, P. V., Moore, R., Hancher, M., Turubanova, S. A., Tyukavina, A., Thau, D., Stehman, S. V., Goetz, S. J., Loveland, T. R., Kommareddy, A., Egorov, A., Chini, L., Justice, C. O., & Townshend, J. R. G. (2013). High-Resolution Global Maps of 21st-Century Forest Cover Change. *Science*, *342*(6160), 850–853. https://doi.org/10.1126/science.1244693

Herdiansyah, H., Negoro, H. A., Rusdayanti, N., & Shara, S. (2020). Palm oil plantation and cultivation: Prosperity and productivity of smallholders. *Open Agriculture*, *5*(1), 617–630. https://doi.org/10.1515/opag-2020-0063

Huete, A., Didan, K., Miura, T., Rodriguez, E. P., Gao, X., Ferreira, L. G. (2002). Overview of the Radiometric and Biophysical Performance of the MODIS Vegetation Indices. *Remote Sensing of the Environment, 83*(1-2), 195-213. https://doi.org/10.1016/S0034-4257(02)00096-2

Intergovernmental Panel on Climate Change. (2023). *IPCC Climate Change 2023 Synthesis Report, Summary for Policymakers*. In H. Lee & J. Romero (Eds). IPCC AR6 Report. https://www.ipcc.ch/report/ar6/syr/downloads/report/IPCC_AR6_SYR_SPM.pdf

mLesage, C., Cifuentes-Espinosa, J., & Feintrenie, L. (2021). Oil palm cultivation in the Americas: review of the social, economic, and environmental conditions of its expansion. *Cahiers Agricultures*, *30*. https://doi.org/10.1051/cagri/2021015

McCarthy, N. (2020). *A Spotlight on Exponential Peruvian Palm Oil Growth ESG Risks for Cargill Subsidiary, Cargill Americas Peru SPL*. Climate Advisors Trust. https://climateadvisers.org/wp-content/uploads/2020/12/Climate-Advisers_A-Spotlight-on-Exponential-Peruvian-Palm-Oil-Growth-2020.pdf

Organismo de Evaluación y Fiscalización Ambiental. (2024, April 11). *Oefa*. gob.pe https://www.gob.pe/oefa

Peru Explorer. (2019, October 3). *Rainforest Facts*. https://www.peru-explorer.com/rainforest_facts.htm

Decreto Legislativo Nº 1090 - Ley Forestal y de Fauna Silvestre. (2008). https://www2.congreso.gob.pe/sicr/cendocbib/con2_uibd.nsf/23C36B7A427AD81D052575C2007FA953/$FILE/D.Leg.1090_Aprueba_Ley_Forestal_Fauna_Silvestre.pdf

mRavikumar, A., Sear, R. R., Cronkleton, P., Silva Menton, M., & Pérez-Ojeda del Arco, M. (2017). Is small-scale agriculture really the main driver of deforestation in the Peruvian Amazon? Moving beyond the prevailing narrative. *Conservation Letters: A journal of the Society for Conservation Biology, 10*(2), 170-177. https://doi.org/10.1111/conl.12264

Rouse, J. W., Haas, R. H., Schell, J. A., & Deering, D. W. (1973) *Monitoring Vegetation Systems in the Great Plains with ERTS (Earth Resources Technology Satellite)*. [Conference Paper] Proceedings of the 3rd Earth Resources Technology Satellite Symposium, Greenbelt, MD, United States. https://ntrs.nasa.gov/citations/19740022614

Shafri, H. Z. M., Hamdan, N., & Saripan, M. I. (2011). Semi-automatic Detection and Counting of Oil Palm Trees from High Spatial Resolution Airborne Imagery. *International Journal of Remote Sensing, 32*(8), 2095-2115. https://doi.org/10.1080/01431161003662928

Smith, T., Traxl, D., & Boers, N. (2022). Empirical evidence for recent global shifts in vegetation resilience. *Nature Climate Change*, *12*(5), 477–484. https://doi.org/10.1038/s41558-022-01352-2

Souza, C. M., Roberts, D. A., & Cochrane, M. A. (2005). Combining spectral and spatial information to map canopy damage from selective logging and forest fires. *Remote Sensing of Environment*, *98*(2–3), 329–343. https://doi.org/10.1016/j.rse.2005.07.013

The Amazon We Want. (2021, November 12). *Amazon Assessment Report 2021*. https://www.theamazonwewant.org/amazon-assessment-report-2021/

Thenkabail, P. S., Stucky, N., Griscom, B. W., Ashton, M. S., Diels, J., van der Meer, B., & Enclona, E. (2004). Biomass estimations and carbon stock calculations in the oil palm plantations of African derived savannas using IKONOS data. *International Journal of Remote Sensing*, *25*(23), 5447–5472. https://doi.org/10.1080/01431160412331291279

Updike, T., & Comp, C. (2010). *Radiometric Use of WorldView-2 Imagery Technical Note*. DigitalGlobe, Inc. https://dg-cms-uploads-production.s3.amazonaws.com/uploads/document/file/104/Radiometric_Use_of_WorldView-2_Imagery.pdf

Villa, L., & Finer, M. (2018, August 27). *MAAP #91: Introducing PeruSAT-1, Peru's new High-resolution Satellite*. Amazon Conservation Association. https://www.maaproject.org/2018/perusat_eng/

Zhu, Z., & Woodcock, C. E. (2014). Continuous change detection and classification of land cover using all available Landsat data. *Remote Sensing of Environment*, *144*, 152–171. https://doi.org/10.1016/j.rse.2014.01.011

9. Appendices

Appendix A: *Overall Deforestation*

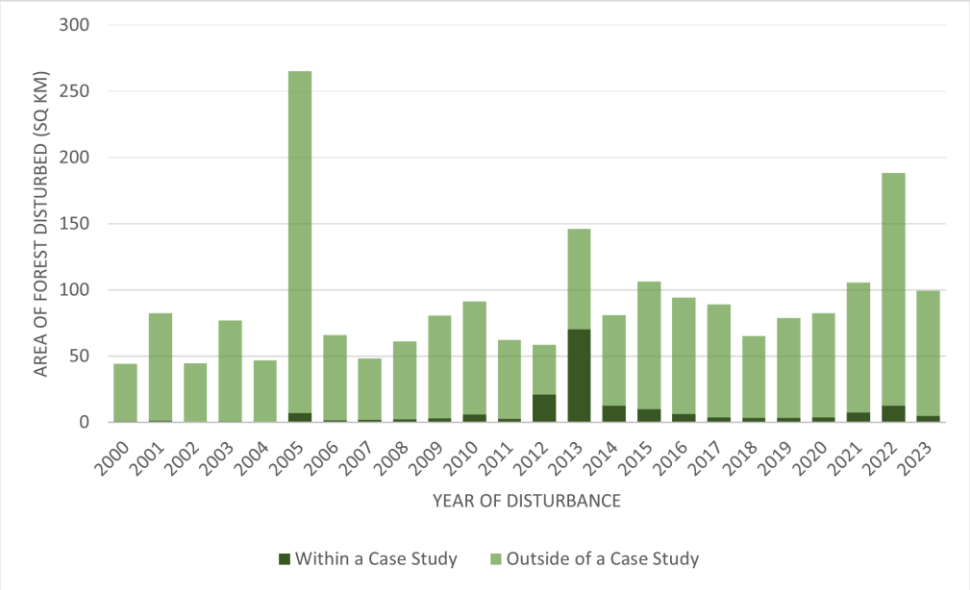

Figure A1. CCDC-SMA bar graph showing the amount of forested area in square kilometers that was disturbed between 2000 and 2023 by the year of disturbance as detected by the tropical CCDC-SMA

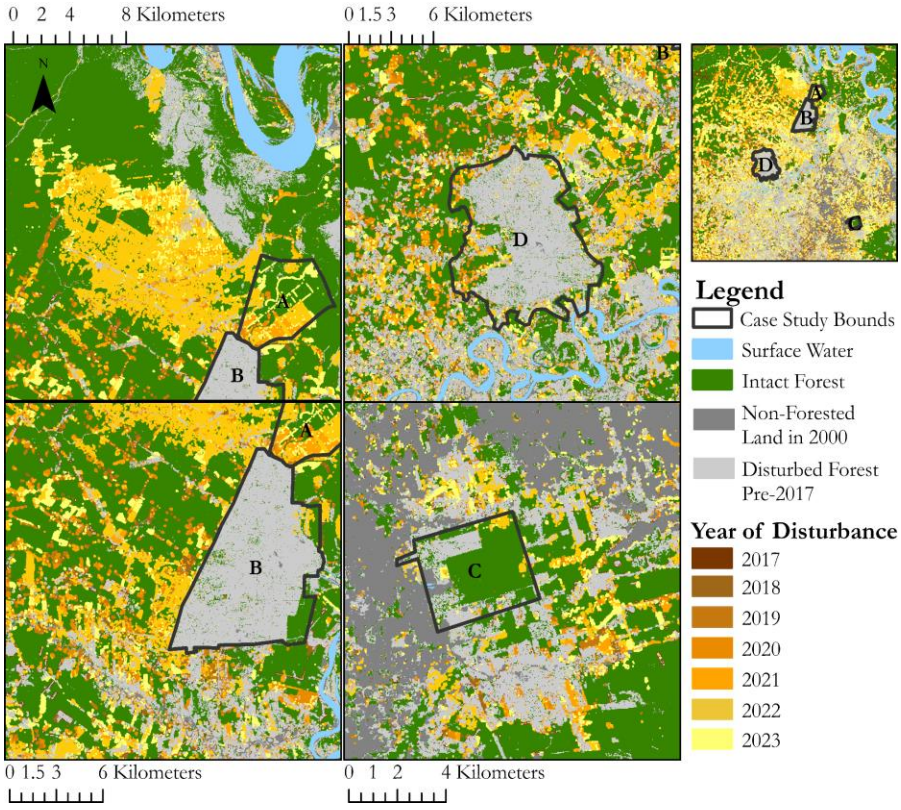

Figure A2. Maps from the CCDC-SMA showing deforestation by year for each case study (A, B, C, and D from left to right) between 2017 – 2023

Appendix B: *PerúSAT-1*

Table B1
PerúSAT-1. Imagery Utilized

File Name	Date	Start Time	Sun Zenith Angle	Earth-Sun Distance	Application
PSH_ORTHO_PER1_20230922151914_SEN_MS_009942.TIF	09/22/2023	15:19:48.92699Z	70.0	1.003212216	Supervised Classification
PSH_ORTHO_PER1_20230922151914_SEN_MS_009324.TIF	09/22/2023	15:19:44.91324Z	70.3	1.003212229	Supervised Classification
PSH_ORTHO_PER1_20180814151704_SEN_MS_000041-022.TIF	08/14/2018	15:17:04.76868Z	49.6	1.012408694	Supervised Classification
PSH_ORTHO_PER1_20221224151236_SEN_MS_000054.TIF	12/24/2022	15:12:36.56068Z	123.9	0.9834276469	Error Assessment
PSH_ORTHO_PER1_20221224151236_SEN_MS_000372.TIF	12/24/2022	15:12:37.59365Z	123.7	0.9834276465	Error Assessment

Table B2
*PerúSAT-1. Solar Spectral Irradiance (EAI) for each of band in W/(m^2*um)*

Band	Solar Spectral Irradiance (W/(m^2*um))
Band 0 – Blue	1982.671954
Band 1 – Green	1826.087443
Band 2 – Red	1540.494123
Band 3 – Alpha/Near Infrared	1094.747446

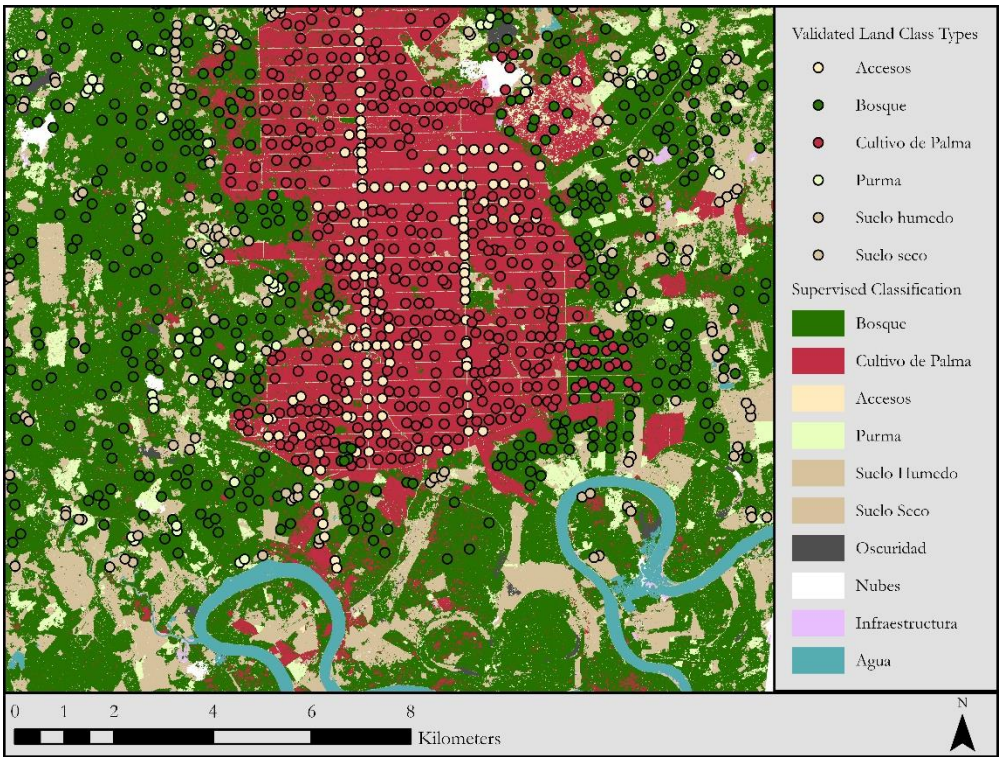

Figure B1. PerúSAT-1. Supervised Classification (2022) with displayed partner provided validation points for accuracy assessment

Table B3

PerúSAT-1 Supervised Classification Error Matrix

Classification Error Matrix	Bosque	Cultivo de Palma	Accesos	Purma	Suelo Humedo	Suelo Seco	Row Total
Bosque	291	31	7	43	11	5	388
Cultivo de Palma	32	313	20	3	3	0	371
Accesos	0	0	67	1	0	3	71
Purma	3	1	2	12	13	9	40
Suelo Humedo	14	0	15	9	46	7	91
Suelo Seco	6	0	25	4	8	33	76
Column Total	346	345	136	72	81	57	1037

Table B4

PerúSAT-1. Accuracy Statistic

Total Pixels Classified	1037
Pixels Correctly Classified	762
Accuracy	73.48%

Table B5

PerúSAT-1. Supervised Classification Translations (Spanish to English)

Spanish Class	**English Class**
Bosque	Forest
Cultivo de Palma	Palm Cultivation (Agriculture)
Accesos	Roads
Purma	Vegetation Regrowth or Low-Lying Vegetation
Suelo Humedo	Moist/Wet Soil
Suelo Seco	Dry Soil
Infraestructura	Infrastructure
Nubes	Clouds
Oscuridad	Shadows
Agua	Water